Nonlinear Dynamics (2026) 114:692
https://doi.org/10.1007/s11071-026-12583-9

RESEARCH

Versatile discrete-time memristive cell

Giacomo Innocenti[1] · Alberto Tesi[1] · Mauro Di Marco[2] · Luca Pancioni[2] · Mauro Forti[2]

Received: 21 February 2026 / Revised: 10 April 2026 / Accepted: 16 April 2026 / Published online: 12 May 2026

Abstract

Over the last decade it has become evident that continuous-time (CT) dynamic circuits containing memristors are capable of exhibiting the coexistence of an "extreme" multitude of different attractors. This distinctive property stems from the so-called *foliation feature*, i.e., the state space of the circuit is composed of infinitely many invariant manifolds to which the dynamics is constrained. More recently, it has been shown that this feature is preserved by the discrete-time (DT) maps derived by discretizing the CT circuit using suitable procedures. In this paper we focus on a CT memristor-capacitor circuit known to possess only equilibrium points as attractors. Specifically, the circuit is a simple memristive cell comprising the parallel interconnection of a capacitor, a passive ideal flux-controlled memristor, and an active resistor. First, the differential equation governing the CT cell is discretized through a foliation-preserving procedure based on a convex combination of Forward and Backward Euler methods. This leads to a (T, λ)-dependent DT map (where T and λ are the discretization time step and the mixing parameter, respectively) that preserves the foliation feature of the CT circuit for any $T > 0$ and any $\lambda \in [0, 1]$. Then, to illustrate the capacity to generate very complex dynamics, we show that these DT maps can exactly reproduce the dynamics of several well-known first-order and second-order chaotic maps (e.g., Circle, Logistic, Hénon and Lozi Maps) on their invariant manifolds, provided that specific embedding conditions involving T, λ, the memristor nonlinear characteristic, and the manifold index are satisfied. Furthermore, under mild assumptions on the parameters of the embedded chaotic map, the (T, λ)-dependent DT map enjoys an intrinsic robustness property that leads to "extreme" multistability phenomena, i.e., the coexistence of infinitely many similar convergent, oscillatory and chaotic behaviors on nearby invariant manifolds. Finally, the Logistic Map is used as a case study to illustrate the DT map derived by solving the embedding conditions, and to discuss robustness of its dynamic behaviors.

Keywords Discrete Memristor · Chaos · Invariant Manifold · Multistability

1 Introduction

Since Williams and his team [1] discovered memristive effects in nanotechnology devices, memristors have been the topic of a literally huge number of contributions in several directions. One direction concerns the study of continuous-time (CT) circuits containing the ideal memristor introduced by L.O. Chua in his seminal paper [2], as the fourth basic passive circuit element. Exploiting memory and nonlinearity, these memristor circuits have been shown to be able to generate extremely rich dynamic behaviors [3–7]. This richness follows from the so-called *foliation feature*, meaning that the state space of the circuit is composed by a continuum of invariant manifolds and the circuit initial conditions determine the index of the manifold where the circuit's dynamics is constrained to lie (see [8, 9] and references therein). This feature ensures an intrinsic robustness of the dynamic behaviors, in the sense that the same type of behavior is displayed on nearby invariant manifolds. This naturally leads to the coexistence of infinitely many convergent, oscillatory and chaotic behaviors, a peculiar property often termed as "extreme" multistability, and to the so-called phenomenon of bifurcations without parameters [10–13].

In the last few years, the development of discrete-time (DT) memristive circuits derived from CT memristive ones has rapidly attracted the interest of researchers. Indeed, DT

✉ Giacomo Innocenti
giacomo.innocenti@unifi.it

[1] Dipartimento di Ingegneria dell'Informazione, Università degli Studi di Firenze, via Santa Marta 3, Firenze 50139, FI, Italy

[2] Dipartimento Ingegneria dell'Informazione e Scienze Matematiche, Università degli Studi di Siena, via Roma, 56, Siena 53100, SI, Italy

maps have some advantages: they can be directly implemented on digital signal processors (see, e.g., [14–16], such as ASICs (Application-Specific Integrated Circuits) and FPGAs (Field-Programmable Gate Arrays)), and their dynamics is much richer than that generated by the CT counterparts, as it was first observed in [17, 18]. The inherent simplicity and high dynamical complexity of DT memristive maps have spurred a rapid proliferation of practical applications. For instance, in [19, 20], chaotic sequences derived from diverse nonlinearities, such as cosine, exponential, and absolute-value functions, are successfully employed for pseudo-random number generation in image encryption and secure communication systems. Similarly, in [21, 22], sine-based architectures incorporating a single n-dimensional memristor or two coupled memristors with a switching mechanism are shown to be able to generate high-complexity suitable for NIST-verified security protocols, along with a low computational overhead optimized for FPGA and DSP (Digital Signal Processor) platforms. The hardware feasibility of specialized models is further explored in [23, 24], where fractional-order differences (Caputo and G–L) and locally active memristors are implemented on FPGA to demonstrate the ease of realizing DT chaotic systems. Discrete memristors have also been considered for enhancing the efficiency of artificial intelligence tasks. For instance, in [25, 26] memristive couplings are used within neural networks to achieve high performance in handwritten letter recognition and color image encryption with relatively simple architectures. Finally, the potential of DT memristive maps for low-cost temporal signal processing is demonstrated in [27, 28] through reservoir computing systems. By leveraging chaotic memristive maps or delay-feedback single-memristor architectures, these models outperform in efficiency traditional recurrent neural networks in classification and multidimensional time-series prediction by significantly reducing training complexity and computational costs.

While it has been shown that DT maps are able to generate very complex dynamics (oscillations, chaos, hyperchaos, ...) and can potentially be exploited for engineering applications, less attention has been devoted to the discretization procedure of CT memristive circuits. Indeed, the procedure typically adopted, which consists of simply applying the Forward Euler integration method to the state equations of the CT circuit, does not in general preserve the foliation feature of the original CT circuits (see, e.g., [29]), thus possibly limiting the coexistence of different attractors. A different discretization procedure for the state-space equations, which preserves the foliation feature independently of the discretization step, has been introduced in [30]. The derived DT maps have been thoroughly investigated in [31, 32], showing also the existence of extreme multistability and bifurcations without parameters. More recently, in [33] this problem has been addressed using a more general procedure within an input-output framework rather than a state-space one. The procedure considers the nonlinear differential equation of the CT circuit and replaces the time-derivative operator with a discretization operator belonging to a very large family which includes classic techniques as well as more complicated methods based on numerical integration and function interpolation. The derived DT maps have been shown to preserve the foliation feature of the original CT circuit for any discretization time step T and for any chosen discretization operator of the family. This allows for the coexistence of many different attractors, as well as extreme multistability, even in case where the memristor characteristic is not of the sine type, as it is usually assumed in the literature. Furthermore, it is shown that non-chaotic CT circuits can become chaotic when the time step T is sufficiently large, a phenomenon termed "computational chaos" by Edward N. Lorenz in [34].

This paper develops a versatile design framework for DT memristive maps by leveraging the input-output discretization procedure introduced in [33]. The study delves into the analysis of this procedure, emphasizing the role played by the discretization operators. The primary objective is to ensure that the resulting discrete models possess two fundamental properties: first, the preservation of the original state-space foliation; and second, the intrinsic robustness of the dynamics on the invariant manifolds against implementation inaccuracies and perturbations. Moreover, the proposed approach offers significant flexibility, as the discretization methods can be configured to precisely select the behavior exhibited on the invariant manifolds. To exemplify this design technique, we specifically consider a CT memristor-capacitor circuit, i.e., a simple memristive cell consisting of the parallel interconnection of a capacitor of capacitance C, a passive ideal flux-controlled memristor, and an active resistor of resistance $-R_A$, $R_A > 0$ (Sect. 2). In [17] it is shown how the DT map, derived by applying the Forward Euler method to the state-space equations of a similar CT memristor-capacitor circuit, is capable of generating very complex dynamics for some suitable time step T, whereas the original CT circuit exhibits simple convergent dynamics. Analogous dynamic behaviors are obtained in [30–32] where the state-space discretization procedure still employs the Forward Euler method, but provides a T-dependent DT map preserving the foliation feature of the original CT circuit for any T.

The objective of this work is to extend the analysis based on the Forward Euler method developed in [30–32] to the general input-output framework introduced in [33]. The aim is to highlight that the choice of the discretization technique plays a crucial role in the design of the DT map and that flexibility in selecting the operator is equally important. To illustrate this result, this paper investigates the DT maps that can be obtained from the previously introduced minimal memristive cell through the class of the discretization

operators generated by any convex combination of Forward and Backward Euler methods (Sect. 3). This yields a map parameterized not only by the discretization time step T, but also by the mixing coefficient λ used for the convex combination, highlighting the relevant role played by the discretization operator in setting up the DT dynamics. Significantly, the foliation feature of the CT memristor-capacitor circuit is preserved for any $T > 0$ and any $\lambda \in [0, 1]$, which is a crucial property for our design procedure. Indeed, not only does it enable the coexistence of multiple attractors without using periodic nonlinearities to generate infinite isolated fixed points, as is necessary when the discretization procedure fails to preserve the foliation, but it is also part of the mechanism that enforces the intrinsic resilience of the designed DT maps.

To investigate the potential of the (T, λ)-dependent DT map in generating complex dynamics, we consider several well-known chaotic first-order and second-order DT maps, i.e., Circle, Cubic, Gaussian, Logistic, Gingerbreadman, Hénon, Holmes and Lozi maps (Sect. 4). For each map, we first compute its input-output difference equation model starting from the state-space one. Then, we check whether the dynamics generated by the input-output DT map can be embedded in the invariant manifold of the (T, λ)-dependent DT map for given R_A and C and by appropriately choosing T, λ, the memristor characteristic and the index ν of the invariant manifold. It turns out that the dynamics of all the considered chaotic maps, except for the Gingerbreadman Map, are exactly reproduced on the invariant manifold related to a specific index ν (Sect. 5). This result demonstrates the flexibility of the proposed approach, which is able to transform a simple CT memristive circuit into a "versatile generator" of dynamically rich DT maps. Furthermore, the chaotic behaviors of these maps are analyzed with respect to variations of the initial conditions (Sect. 6), showing that, under mild assumptions on the parameters of the map to be embedded, they enjoy robustness, i.e., attractors of the same type are displayed on nearby invariant manifolds. This resilience is a highly desirable property, since it guarantees that the characteristics of the embedded dynamics are preserved even in the presence of small inaccuracies, possibly coming from software and hardware implementation. The well-known Logistic Map is finally employed to illustrate and discuss in detail the discretization procedure as well as the robustness features of the dynamic behaviors of the DT map derived via the embedding conditions (Sect. 7). Some concluding remarks end the paper in Sect. 8.

1.1 Notation

- $\mathbb{R}$, $\mathbb{Z}$, $\mathbb{Z}_+$: real set, integer set, non-negative integer set
- $t \in \mathbb{R}$, $k \in \mathbb{Z}$: continuous-time (CT) variable, discrete-time (DT) variable

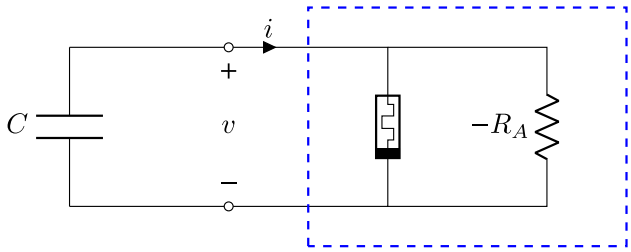

Fig. 1 The CT memristive cell composed by a mesh with a capacitor of capacitance $C > 0$ and the parallel interconnection (dashed blue box) between a passive ideal memristor and a resistor with a negative resistance $-R_A$, $R_A > 0$

- $f(t)$, f_k: real-valued CT function of $t \in \mathbb{R}$, real-valued DT sequence of $k \in \mathbb{Z}$
- $\mathcal{D}$: time-derivative operator $\frac{d}{dt}$
- $\mathcal{D}^i f(t)$: value assumed by the i-th time-derivative of function f at time t
- H: nonlinear function of the constitutive relation of the memristor
- H': derivative of function H (memductance of the memristor)
- $\mathcal{C}^1(\mathbb{R})$: class of functions continuous on $\mathbb{R}$ up to the first derivative
- T: discretization time step
- h_T: CT T-ahead shift operator, i.e., $h_T f(t) = f(t + T)$
- h: DT one-step-ahead shift operator, i.e., $h f_k = f_{k+1}$
- $\Delta(T, h_T)$: CT discretization operator
- $\Delta(T, h)$: DT discretization operator

2 The CT memristive cell

Consider the CT memristor-capacitor circuit depicted in Fig. 1, i.e., a simple memristive cell made of a mesh featuring a capacitor, whose voltage, current, and capacitance are v, i, and $C > 0$, and the parallel interconnection of a passive ideal flux-controlled memristor and an active resistor, whose resistance is $-R_A$, $R_A > 0$. Notice that such a configuration is the standard way to model "locally active" memristors, as illustrated in the seminal paper [3], since the ideal memristor is intrinsically a passive device. Denoting as v_M and i_M the voltage and current of the memristor, the passive ideal flux-controlled memristor is defined by the constitutive relation $q = H(\varphi)$, where $q(t) = \int_{-\infty}^{t} i_M(\tau) d\tau$ and $\varphi(t) = \int_{-\infty}^{t} v_M(\tau) d\tau$ are the charge and the flux, respectively, and $H : \mathbb{R} \to \mathbb{R}$ is a function that is continuously differentiable almost everywhere on the real axis and such that $H(0) = 0$. By differentation, the memristor satisfies

$$\begin{cases} i_M = H'(\varphi) v_M \\ \mathcal{D}\varphi = v_M \end{cases},$$

where $H'(\varphi)$ is known as the memductance. Since the memristor is passive, we have that $H(\varphi)$ is a non-decreasing nonlinear function [2]. The second equation is termed memristor state equation and it defines how the state variable (the flux) depends on the voltage, while the first equation shows that the memristor current-voltage characteristic amounts to a state-dependent Ohm's law. Since $v = v_M$ and $i = i_M - 1/R_A v_M$, we have that

$$i = \left(H'(\varphi) - \frac{1}{R_A} \right) v \, ,$$

which shows that the memristive cell can be locally active if $1/R_A$ is greater than $H'(\varphi)$ on some intervals of φ.

By selecting the memristor flux φ and the capacitor voltage v as state variables, we get that the circuit dynamics obeys the following state-space equations

$$\begin{cases} \mathcal{D}\varphi = v \\ \mathcal{D}v = \frac{1}{R_A C} v - \frac{1}{C} H'(\varphi) v \, . \end{cases} \tag{1}$$

Note that the above system possesses infinitely many equilibrium points given by $v = 0$ and $\varphi \in \mathbb{R}$. System (1) admits an equivalent input-output representation via the following second-order differential equation

$$\mathcal{D}^2\varphi - \frac{1}{R_A C}\mathcal{D}\varphi + \frac{1}{C} H'(\varphi)\mathcal{D}\varphi = 0 \tag{2}$$

and the solution $(\varphi(t), v(t))$, $t \geq 0$, of (1) with initial condition $(\varphi(0), v(0)) = (\varphi_0, v_0)$ can be obtained by solving (2) with initial conditions $(\varphi(0), \mathcal{D}\varphi(0)) = (\varphi_0, v_0)$. Since $H'(\varphi)\mathcal{D}\varphi = \mathcal{D}H(\varphi)$, (2) can be rewritten as

$$\mathcal{D}\left(\mathcal{D}\varphi - \frac{1}{R_A C}\varphi + \frac{1}{C} H(\varphi) \right) = 0 \, . \tag{3}$$

The above equation highlights the existence of a first integral, i.e.

$$\mathcal{D}\varphi - \frac{1}{R_A C}\varphi + \frac{1}{C} H(\varphi) = \mu \tag{4}$$

where $\mu \in \mathbb{R}$ depends on the initial conditions as follows

$$\mu = v_0 - \frac{1}{R_A C}\varphi_0 + \frac{1}{C} H(\varphi_0) \, . \tag{5}$$

The existence of the first integral implies that, as expected, the circuit enjoys the *foliation feature* [8, 9], i.e., the state space of the circuit is composed by a continuum of invariant manifolds where the circuits dynamics is constrained to lie. Indeed, consider the one-dimensional manifold

$$\mathcal{M}_\mu = \left\{ \varphi \in \mathbb{R}, \mathcal{D}\varphi \in \mathbb{R} : \right.$$

$$\left. \mathcal{D}\varphi = \frac{1}{R_A C}\varphi - \frac{1}{C} H(\varphi) + \mu \right\} \, , \tag{6}$$

where $\mu \in \mathbb{R}$ is usually referred to as the manifold index. It can be easily seen that the state space with coordinates $(\varphi, \mathcal{D}\varphi = v)$ is completely covered by the family of manifolds $\{\mathcal{M}_\mu, \ \mu \in \mathbb{R}\}$.

Furthermore, notice that the solution $(\varphi(t), v(t))$, $t \geq 0$, of (1) with initial condition $(\varphi(0), v(0)) = (\varphi_0, v_0)$ can be obtained by first solving for $\varphi(t)$, $t \geq 0$, the first-order differential equation (4) with μ as in (5) and initial condition $\varphi(0) = \varphi_0$ and then obtaining $v(t) = \mathcal{D}\varphi(t)$ directly from (6), i.e., $v(t) = \varphi(t)/(R_A C) - H(\varphi(t))/C + \mu$, $t \geq 0$. This clearly implies that manifold $\mathcal{M}_\mu$ is (forward) invariant, since for $t \geq 0$ the solution is constrained to evolve on it.

Remark 1 The first-order differential equation (4) is a reduced order model of the second-order state equations (1), i.e., the dynamics of the CT memristive cell of Fig.1 is completely characterized by the dynamic behaviors obtained from (4) by varying $\mu \in \mathbb{R}$. Even if these behaviors clearly depend on C, R_A and the function H, they are generated by the first-order differential (4) and hence we can conclude that the circuit can have only stable equilibrium points as attractors. Note that the equilibrium points on the invariant manifold $\mathcal{M}_\mu$ are such that $v = 0$ and $\varphi = \bar{\varphi}$, where $\bar{\varphi}$ is a solution of $R_A H(\bar{\varphi}) - \bar{\varphi} = R_A C \mu$. Furthermore, except for singular cases where a bifurcation occurs, the stable equilibrium points remain stable for small variations of the manifold index μ (see Sect. 7). This implies the same convergent behavior is displayed on nearby manifolds, thus showing an intrinsic robustness of the attractors of the memristive cell.

3 The DT memristive cell

In this section, we derive a DT model of the CT memristive cell of Fig. 1 by appropriately tailoring the general procedure proposed in [33] that has been shown to preserve the foliation feature for any discretization time step T.

The first step consists in determining a suitable CT discretization operator that locally approximates the time-derivative operator $\mathcal{D}$. Local approximations of $\mathcal{D}$ can be designed exploiting the CT T-ahead shift operator h_T. Indeed, it is known (see, e.g., Sections 9.1.1 and 9.1.2 of [33]) that for any given $T > 0$ the Forward Euler method provides the approximate relation

$$\mathcal{D} \approx \Delta_{FE}(T, h_T) \triangleq \frac{h_T - 1}{T} \, , \tag{7}$$

while the Backward Euler method is such that:

$$\mathcal{D} \approx \Delta_{BE}(T, h_T) \triangleq \frac{h_T - 1}{T h_T} . \tag{8}$$

In this paper we devise a more flexible and general CT discretization operator by using a convex combination of (7) and (8), i.e.

$$\begin{aligned}\Delta_A(T, h_T; \lambda) &\triangleq \lambda \frac{h_T - 1}{T} + (1 - \lambda)\frac{h_T - 1}{T h_T} \\ &= \frac{h_T - 1}{T} \cdot \frac{\lambda h_T + 1 - \lambda}{h_T}\end{aligned} \tag{9}$$

with $0 \leq \lambda \leq 1$. Note that the discretization operator (9) depends on two parameters, namely T and λ. Furthermore, it enjoys the properties given below.

Proposition 1

1) The CT discretization operator $\Delta_A(T, h_T; \lambda)$ satisfies

$$\lim_{T \to 0^+} [\Delta_A(T, h_T; \lambda) f(t)] = \mathcal{D} f(t) , \quad \forall t \in \mathbb{R} \tag{10}$$

for any function of time $f(t)$ that is t-differentiable (almost) everywhere and for any $\lambda \in [0, 1]$.

2) For any function $f(t)$ constant over time, i.e., $f(t) = K$, $K \in \mathbb{R}$, we have

$$\Delta_A(T, h_T; \lambda) f(t) = 0 , \forall T > 0, \forall \lambda \in [0, 1] .$$

3) By construction we have that $\Delta_A(T, h_T; 0) = \Delta_{BE}(T, h_T)$ and $\Delta_A(T, h_T; 1) = \Delta_{FE}(T, h_T)$, while

$$\Delta_A(T, h_T; 1/2) = \frac{h_T^2 - 1}{2 T h_T}$$

corresponds to the Midpoint Rule [35].

In the second step we substitute the time derivative operator $\mathcal{D}$ with the discretization operator $\Delta_A(T, h_T; \lambda)$ in the differential equation (3), thus obtaining a local approximation $\varphi_a(t)$ of the flux the CT memristive cell that satisfies:

$$\begin{aligned}\Delta_A(T, h_T; \lambda)\Bigg(\Delta_A(T, h_T; \lambda)\varphi_a(t) - \frac{1}{R_A C}\varphi_a(t) \\ + \frac{1}{C} H(\varphi_a(t))\Bigg) = 0\end{aligned} \tag{11}$$

for all $t \geq 0$. The final step consists in deriving a DT map from (11) by defining $\varphi_k = \varphi_a(t)|_{t=kT} = \varphi_a(kT)$, $k \in \mathbb{Z}$ and substituting h_T with the DT one-step operator h in (9), thus getting the following DT operator:

$$\begin{aligned}\Delta(T, h; \lambda) &\triangleq \frac{h - 1}{T} \cdot \frac{\lambda h + 1 - \lambda}{h} \\ &= \frac{\lambda h^2 + (1 - 2\lambda)h + \lambda - 1}{hT} .\end{aligned} \tag{12}$$

The final result is a DT model described by the following difference equation

$$\Delta(T, h; \lambda)\left(\Delta(T, h; \lambda)\varphi_k - \frac{1}{R_A C}\varphi_k + \frac{1}{C} H(\varphi_k)\right) = 0 . \tag{13}$$

Indeed, this model is the DT counterpart of the CT input-output model (3). The relationship between the solution $\varphi(t)$ of the CT model and the sequence φ_k solving (13) is discussed in Remark 2 below.

It can be readily verified that (13) is an explicit fourth-order difference equation for $\lambda \in [0, 1)$ (resp. second-order for $\lambda = 1$) that relates φ_{k+4} with φ_{k+3}, φ_{k+2}, φ_{k+1}, and φ_k (resp. φ_{k+2} with φ_{k+1}, and φ_k). A state equation representation of the DT model can be readily obtained for the difference equation by using $\varphi_{k+3}, \varphi_{k+2}, \varphi_{k+1}$, and φ_k as state variables (resp. φ_{k+1}, and φ_k). Now, we show that it enjoys the foliation feature. To see this, consider the sequence z_k, $k \in \mathbb{Z}$, defined as

$$z_k \triangleq \Delta(T, h; \lambda)\varphi_k - \frac{1}{R_A C}\varphi_k + \frac{1}{C} H(\varphi_k) \tag{14}$$

and observe that, according to (12), any constant sequence $z_k = \nu \in \mathbb{R}$, $k \in \mathbb{Z}$, belongs to the kernel of $\Delta(T, h; \lambda)$, i.e.,

$$\Delta(T; \lambda) z_k = 0 , \quad \forall k \in \mathbb{Z}, \forall \lambda \in [0, 1] .$$

This implies that for any $\nu \in \mathbb{R}$ the equation

$$\Delta(T, h; \lambda)\varphi_k - \frac{1}{R_A C}\varphi_k + \frac{1}{C} H(\varphi_k) = \nu \tag{15}$$

represents an invariant manifold of the DT model (13). By replacing $\Delta(T, h; \lambda)$ with its expression in (12), the expanded form of (15) becomes

$$\begin{aligned}&\frac{\lambda}{T}\varphi_{k+2} + \left((1 - 2\lambda)\frac{1}{T} - \frac{1}{R_A C}\right)\varphi_{k+1} \\ &\quad + \frac{\lambda - 1}{T}\varphi_k + \frac{1}{C} H(\varphi_{k+1}) = \nu ,\end{aligned} \tag{16}$$

that amounts to a second-order difference equation depending on the circuit parameters C, R_A, H, the time step T, the parameter λ mixing Forward and Backward Euler methods, and the parameter ν that, as for the CT case, represents the manifold index. It is given by

$$\begin{aligned}\nu = &\frac{\lambda}{T}\varphi_2 + \left((1 - 2\lambda)\frac{1}{T} - \frac{1}{R_A C}\right)\varphi_1 \\ &+ \frac{\lambda - 1}{T}\varphi_0 + \frac{1}{C} H(\varphi_1) ,\end{aligned} \tag{17}$$

where φ_0, φ_1, and φ_2 are the initial conditions of the sequence φ_k. Nonetheless, it is important to stress that in general ν is unrelated to its CT counterpart μ. In the next sections, we show that the difference equation (16) can mimic well-known chaotic maps by appropriately choosing the shape of the function H, i.e., the constitutive relation of the passive memristor, the manifold index ν, and the values of $T \in \mathbb{R}$ and $\lambda \in [0, 1]$.

Some final remarks are in order.

Remark 2 Notice that $\varphi_k = \varphi_a(kT)$ is only an approximation of the sequence $\varphi(kT) = \varphi(t)|_{t=kT}$ since the solution $\varphi_a(t)$ of (11) differs from the solution $\varphi(t)$ of (3), even if $\varphi(0) = \varphi_a(0)$. In general, this difference may be taken small by using sufficiently small T and employing suitable numerical integration algorithms that adjust dynamically T [36, 37]. On the other hand, in the next sections we show that the non-chaotic CT memristive cell becomes chaotic if T is sufficiently large, a phenomenon which is referred to as computational chaos by Lorenz in [34].

Remark 3 When $\lambda = 0$, i.e., the Backward Euler Method case, model (16) boils down to the implicit first-order difference equation

$$\left(1 - \frac{T}{R_A C}\right)\varphi_{k+1} - \varphi_k + \frac{T}{C}H(\varphi_{k+1}) = T\nu \tag{18}$$

where φ_{k+1} cannot be expressed as an explicit function of φ_k. When $\lambda = 1$, , i.e., the Forward Euler Method case, model (16) reduces to the following explicit first-order difference equation

$$\frac{1}{T}\varphi_{k+2} - \left(\frac{1}{T} + \frac{1}{R_A C}\right)\varphi_{k+1} + \frac{1}{C}H(\varphi_{k+1}) = \nu\ .$$

Via a proper time-shift, we get the standard form of the difference equation

$$\varphi_{k+1} = \left(1 + \frac{T}{R_A C}\right)\varphi_k - \frac{T}{C}H(\varphi_k) + T\nu\ , \tag{19}$$

where the index manifold ν is given by

$$\nu = \frac{1}{T}\varphi_1 - \left(\frac{1}{T} + \frac{1}{R_A C}\right)\varphi_0 + \frac{1}{C}H(\varphi_0)\ , \tag{20}$$

with φ_0 and φ_1 being the initial conditions of the sequence φ_k.

Remark 4 Notice that the DT model (13) possesses a more general form of invariant manifolds. Indeed, from (14) and (12) it follow that we can rewrite (13) as

$$0 = \Delta(T;\lambda)z_k = \frac{h-1}{hT}(\lambda z_{k+1} + (1-\lambda)z_k)\ ,$$

which implies that the sequence $\lambda z_{k+1} + (1-\lambda)z_k$ is constant for all $k \in \mathbb{Z}$. Taking into account that the left hand side of (16) is the expanded form of z_k, the fourth-dimensional invariant manifolds of (13) assume the following general form

$$\mathcal{M}_\nu = \Bigg\{\varphi_k, \varphi_{k+1}, \varphi_{k+2}, \varphi_{k+3} : \lambda\Bigg(\frac{\lambda}{T}\varphi_{k+3} \tag{21}$$

$$+ \Big((1-2\lambda)\frac{1}{T} - \frac{1}{R_A C}\Big)\varphi_{k+2} + \frac{\lambda-1}{T}\varphi_{k+1} \tag{22}$$

$$+ \frac{1}{C}H(\varphi_{k+2})\Bigg) \tag{23}$$

$$+ (1-\lambda)\Bigg(\frac{\lambda}{T}\varphi_{k+2} + \Big((1-2\lambda)\frac{1}{T} - \frac{1}{R_A C}\Big)\varphi_{k+1} \tag{24}$$

$$+ \frac{\lambda-1}{T}\varphi_k + \frac{1}{C}H(\varphi_{k+1})\Bigg) = \nu\Bigg\}\ , \tag{25}$$

where the manifold index ν can be computed via the initial conditions φ_i, $i = 0, 1, 2, 3$. Notice that the general form of the invariant manifolds is characterized by a third-order difference equation. However, since the chaotic maps considered in Sect. 4 are of first-order or second-order, we only exploit the more simple invariant manifolds (16) to mimic their dynamics.

4 Chaotic maps

In this Section we consider a number of well-known first-order and second-order chaotic maps. The state equations of these first-order and second-order maps are reported in the first column of Table 1 and Table 2, respectively, together with the usual values of the parameters for which the maps exhibit chaotic behaviors [38, 39]. We first show that these chaotic maps admit an explicit difference model sharing the same structure of the explicit difference equation models (19) and (16). This input-output form makes easier to derive conditions ensuring that the chaotic maps can be embedded in the invariant manifolds of the DT input-output model (13).

It can be shown that each second-order map in Table 2 can be equivalently described by an explicit difference equation model of the following form

$$z_{k+2} + \sigma_1(\varrho)z_{k+1} + \sigma_0(\varrho)z_k + \Phi(z_{k+1};\varrho) + \gamma(\varrho) = 0\ , \tag{26}$$

where z_k is the generic DT variable and $\varrho \in \mathbb{R}^m$, $m \geq 1$, is the vector of the parameters of the map. The functions σ_0, σ_1, and γ are the coefficients of the model depending on ϱ, while Φ denotes the purely nonlinear function of the map. The cases where the derivation of the difference equation model from the state equations is not trivial are dealt with in Appendix 9.

Similarly, it can be readily verified that each first-order map in Table 1 obeys an explicit difference equation given by

$$z_{k+1} + \sigma_0(\varrho) z_k + \Phi(z_k; \varrho) + \gamma(\varrho) = 0 \,. \tag{27}$$

The specific expressions of z_k and ϱ are reported for each map in the second column of Tables 1 and 2.

The DT cell with manifold dynamics described by the explicit difference equations (16) and (19) can mimic the dynamics of the chaotic maps. Specifically, in the case of second-order maps (26) we employ (16) with $\lambda \in (0, 1)$. First, by adding and subtracting the term $\alpha \frac{T}{C} \varphi_k$ where $\alpha \in \mathbb{R}$ is an auxiliary parameter, (16) is rewritten as

$$\begin{aligned} &\varphi_{k+2} + \left(\frac{1-2\lambda}{\lambda} - \frac{T}{\lambda R_A C} - \alpha \frac{T}{\lambda C} \right) \varphi_{k+1} \\ &\quad + \frac{\lambda - 1}{\lambda} \varphi_k + \frac{T}{\lambda C} \left(H(\varphi_{k+1}) + \alpha \varphi_{k+1} \right) - \frac{T}{\lambda} \nu = 0 \,. \end{aligned} \tag{28}$$

Observe that any choice of $\alpha \in \mathbb{R}$ changes the slope of the term containing the nonlinear function H. Rewriting more compactly the coefficient of φ_{k+1} in (28), we get the following final form of (16)

$$\begin{aligned} &\varphi_{k+2} + \left(\frac{1-2\lambda}{\lambda} - \frac{(1+\alpha R_A) T}{\lambda R_A C} \right) \varphi_{k+1} + \frac{\lambda - 1}{\lambda} \varphi_k \\ &\quad + \frac{T}{\lambda C} \left(H(\varphi_{k+1}) + \alpha \varphi_{k+1} \right) - \frac{T}{\lambda} \nu = 0 \,. \end{aligned} \tag{29}$$

Then, by setting $z_k = \varphi_k$, the conditions to embed (26) in the invariant manifolds of the DT model become

$$\begin{cases} \sigma_1(\varrho) = \frac{1-2\lambda}{\lambda} - \frac{(1+\alpha R_A) T}{\lambda R_A C} \\ \sigma_0(\varrho) = \frac{\lambda - 1}{\lambda} \\ \Phi(\varphi; \varrho) = \frac{T}{\lambda C} \left(H(\varphi) + \alpha \varphi \right) \\ \gamma(\varrho) = -\frac{T}{\lambda} \nu \,. \end{cases} \tag{30}$$

Notice that since $\lambda \in (0, 1)$ the second equation limits the possible values of the coefficient σ_0 .

In the case of first-order maps, we use model (19) with $\lambda = 1$, i.e., the DT operator is the Forward Euler method. Using the additional parameter α, after some straightforward manipulations, (19) boils down to

$$\begin{aligned} &\varphi_{k+1} - \left(1 + (1 + \alpha R_A) \frac{T}{R_A C} \right) \varphi_k \\ &\quad + \frac{T}{C} \left(H(\varphi_k) + \alpha \varphi_k \right) - T \nu = 0 \,. \end{aligned} \tag{31}$$

Hence, the chaotic maps (27) that can be embedded should fulfill the following conditions:

$$\begin{cases} \sigma_0(\varrho) = -\left(1 + (1 + \alpha R_A) \frac{T}{R_A C} \right) \\ \Phi(\varphi; \varrho) = \frac{T}{C} \left(H(\varphi) + \alpha \varphi \right) \\ \gamma(\varrho) = -T \nu \,. \end{cases} \tag{32}$$

5 Embedding chaotic maps into the manifolds of the DT memristive cell

In this section we investigate how the dynamics on the manifolds (19) and (16) of the DT memristive cell (13) can be tuned to mimic the chaotic maps. Specifically, for the first-order maps reported in Table 1, in Sect. 5.1 we first solve for α, H, and ν the embedding equations (32) and then look for conditions on T that ensure passivity of the memristor, i.e., $H'(\varphi) \geq 0$, $\forall \varphi \in \mathbb{R}$. In Sect. 5.2, the same approach is applied to the second-order maps reported in Table 2 with the difference that we first have to check if the second equation in (30) is solved from some $\lambda \in (0, 1)$ and then proceed as in the first-order case. If such a λ does not exist, as in the case of the Gingerbreadman Map, than that chaotic map cannot be embedded on the manifolds (16) of the DT memristive cell (13).

5.1 Derivation of embedding conditions for first-order maps

In this Section, for each first-order map of Table 1 we consider the relative difference equation reported in the second column and identify the specific expression of σ_0, Φ, and γ. Then, we apply the approach outlined above to derive the embedding conditions, which are reported in the third column of Table 1.

5.1.1 Circle Map

The Circle Map obeys the following first-order difference equation

$$z_{k+1} - z_k - \frac{K}{2\pi} \sin(2\pi z_k) - \Omega = 0 \tag{33}$$

and hence we have $\sigma_0 = -1$, $\Phi = -(K/2\pi) \sin(2\pi)\varphi$, $\gamma = -\Omega$. Solving for the auxiliary parameter α the first equation of (32) yields $\alpha = -1/R_A$. Then, it turns out that the remaining equations are solved for

$$H(\varphi) = -\frac{KC}{2\pi T} \sin(2\pi\varphi) + \frac{1}{R_A} \varphi \,, \quad \nu = \frac{1}{T} \Omega \,.$$

Table 1 List of first-order chaotic maps

State Space Model	Input-output Difference Equation	Embedding Conditions
Circle Map [38]		
$\theta_{k+1} = \theta_k + \Omega + \frac{K}{2\pi}\sin(2\pi\theta_k)$ $\Omega = 0.5$ $K = 2$	$z_{k+1} - z_k - \Omega - \frac{K}{2\pi}\sin(2\pi z_k) = 0$ $z_k \triangleq \theta_k$ $\varrho \triangleq \begin{bmatrix}\Omega \\ K\end{bmatrix}$	$\lambda = 1$ $T \geq K R_A C$ $H(\varphi) = \frac{1}{R_A}\varphi - \frac{KC}{2\pi T}\sin(2\pi\varphi)$ $\nu = \frac{1}{T}\Omega$
Cubic map [38]		
$x_{k+1} = a x_k (1 - x_k^2)$ $a = 3$	$z_{k+1} - a z_k + a z_k^3 = 0$ $z_k \triangleq x_k$ $\varrho \triangleq a$	$\lambda = 1$ $T \geq (a-1) R_A C$ $H(\varphi) = a\frac{C}{T}\varphi^3 + \left(\frac{1}{R_A} + (1-a)\frac{C}{T}\right)\varphi$ $\nu = 0$
Gaussian Map [39]		
$x_{k+1} = e^{-b x_k^2} + c$ $b = 7.5$ $c = -0.6$	$z_{k+1} - e^{-b z_k^2} - c = 0$ $z_k \triangleq x_k$ $\varrho \triangleq \begin{bmatrix}b \\ c\end{bmatrix}$	$\lambda = 1$ $T \geq \left(\sqrt{\frac{2b}{e}} - 1\right) R_A C$ $H(\varphi) = \frac{C}{T} e^{-b\varphi^2} + \left(\frac{C}{T} + \frac{1}{R_A}\right)\varphi$ $\nu = \frac{1}{T} c$
Logistic Map [38]		
$x_{k+1} = a x_k (1 - x_k)$ $a = 4$	$z_{k+1} - a z_k + a z_k^2 = 0$ $z_k \triangleq x_k$ $\varrho \triangleq a$	$\lambda = 1$ $T \geq (a(1-2M_i) - 1) R_A C$ $H(\varphi) = a\frac{C}{T}\varphi^2 + \left(\frac{1}{R_A} + (1-a)\frac{C}{T}\right)\varphi$ $\nu = 0$

The first column contains the standard state equations of the map together with the typical values of its parameters; the second column reports the difference equation model of the map together with the parameter vector ϱ; the third column contains the conditions for embedding the map in the invariant manifolds (19) of the DT memristive cell. In the case of the Logistic map H should be replaced by H_p in (40), while M_i is the lower bound of the considered chaotic motions $\{\varphi_k,\ k \in \mathbb{Z}_+\}$, i.e., $\varphi_k \geq M_i, \forall k \in \mathbb{Z}_+$

respectively. Finally, since

$$H'(\varphi) = -K\frac{C}{T}\cos(2\pi\varphi) + \frac{1}{R_A}\,,$$

the condition for the memristor to be passive requires that T satisfies

$$T \geq K R_A C\,.$$

5.1.2 Cubic map

The Cubic Map is described by the following difference equation

$$z_{k+1} - a z_k + a z_k^3 = 0\,, \tag{34}$$

that implies $\sigma_0 = -a$, $\Phi = a\varphi^3$, and $\gamma = 0$. Hence, equations (32) hold if α, H, and ν are given by

$$\alpha = (a-1)\frac{C}{T} - \frac{1}{R_A}\,,$$
$$H(\varphi) = a\frac{C}{T}\varphi^3 + \left(\frac{1}{R_A} + (1-a)\frac{C}{T}\right)\varphi\,,$$
$$\nu = 0\,,$$

respectively. Since

$$H'(\varphi) = 3a\frac{C}{T}\varphi^2 + \frac{1}{R_A} + (1-a)\frac{C}{T}\,,$$

the memristor is passive if T is such that

$$T \geq (a-1) R_A C\,.$$

5.1.3 Gaussian Map

The difference equation of the map is

$$z_{k+1} - e^{-b z_k^2} - c = 0$$

and hence we have $\sigma_0 = 0$, $\Phi = -e^{-b\varphi^2}$, and $\gamma = -c$. It turns out that equations (32) are solved for

$$\alpha = -\frac{C}{T} - \frac{1}{R_A}\,,$$
$$H(\varphi) = -\frac{C}{T}e^{-b\varphi^2} + \left(\frac{C}{T} + \frac{1}{R_A}\right)\varphi\,,$$

Table 2 List of second-order chaotic maps

State Space Model	Input-output Difference Equation	Embedding Conditions
Gingerbreadman Map [38]		
$\begin{cases} x_{k+1} = 1 + \lvert x_k\rvert - y_k \\ y_{k+1} = x_k \end{cases}$	$z_{k+2} + z_k - \lvert z_{k+1}\rvert - 1 = 0$ $z_k \triangleq y_k$	None
Hénon Map [38]		
$\begin{cases} x_{k+1} = 1 - ax_k^2 + y_k \\ y_{k+1} = bx_k \end{cases}$ $a = 1.4$ $b = 0.3$	$z_{k+2} - bz_k + \frac{a}{b} z_{k+1}^2 - b = 0$ $z_k \triangleq y_k$ $\varrho \triangleq \begin{bmatrix} a \\ b \end{bmatrix}$	$\lambda = \frac{1}{1+b} \implies b > 0$ $T \geq \frac{1}{1+b}\left(\frac{2a}{b} M_i - 1 + b\right) R_A C$ $H(\varphi) = a\frac{C}{T}\varphi^2 + \left(\frac{C}{T} + \frac{1}{R_A}\right)\varphi$ $\nu = \frac{b}{(1-b)T}$
Holmes Map [38]		
$\begin{cases} x_{k+1} = y_k \\ y_{k+1} = -bx_k + dy_k - y_k^3 \end{cases}$ $b = 0.2$ $d = 2.77$	$z_{k+2} - dz_{k+1} + bz_k + z_{k+1}^3 = 0$ $z_k \triangleq x_k$ $\varrho \triangleq \begin{bmatrix} b \\ d \end{bmatrix}$	$\lambda = \frac{1}{1-b} \implies b < 0$ $T \geq \frac{d-b-1}{1-b} R_A C$ $H(\varphi) = d\frac{C}{T}\varphi^2 + \left(\frac{C}{T} + \frac{1}{R_A}\right)\varphi$ $\nu = 0$
Lozi Map [38]		
$\begin{cases} x_{k+1} = 1 - a\lvert x_k\rvert + y_k \\ y_{k+1} = bx_k \end{cases}$ $a = 1.7$ $b = 0.5$	$z_{k+2} - bz_k + \frac{a}{b}\lvert z_{k+1}\rvert - b = 0$ $z_k \triangleq y_k$ $\varrho \triangleq \begin{bmatrix} a \\ b \end{bmatrix}$	$\lambda = \frac{1}{1+b} \implies b > 0$ $T \geq \frac{1+a-b^2}{b(1+b)} R_A C$ $H(\varphi) = \frac{C}{T}\frac{a}{(1+b)b}\lvert\varphi\rvert + \left(\frac{C}{T}\frac{1-b}{1+b} + \frac{1}{R_A}\right)\varphi$ $\nu = \frac{b}{(1-b)T}$

The first column contains the standard state equations of the map together with the typical values of its parameters; the second column reports the difference equation model of the map together with the parameter vector ϱ; the third column contains the conditions for embedding the map in the invariant manifolds (16) of the DT memristive cell. In the case of the Hénon map H should be replaced by H_p in (40), while M_i is the lower bound of the considered chaotic motions $\{\varphi_k,\ k \in \mathbb{Z}_+\}$, i.e., $\varphi_k \geq M_i$, $\forall k \in \mathbb{Z}_+$

$$\nu = \frac{1}{T} c \, .$$

Since

$$H'(\varphi) = 2b\frac{C}{T}\varphi e^{-b\varphi^2} + \frac{C}{T} + \frac{1}{R_A} \, ,$$

it follows that the memristor is passive if T satisfies

$$T \geq \left(\sqrt{\frac{2b}{e}} - 1\right) R_A C \, .$$

5.1.4 Logistic Map

The logistic Map is described by the following difference equation

$$z_{k+1} - az_k + az_k^2 = 0 \, , \tag{35}$$

that leads to $\sigma_0 = -a$, $\Phi = a\phi^2$, and $\gamma = 0$. It can be verified that equations (32) are satisfied if α, H, and ν are given by

$$\alpha = (a-1)\frac{C}{T} - \frac{1}{R_A} \, , \tag{36}$$

$$H(\varphi) = a\frac{C}{T}\varphi^2 + \left(\frac{1}{R_A} + (1-a)\frac{C}{T}\right)\varphi \, , \tag{37}$$

$$\nu = 0 \, , \tag{38}$$

respectively. Notice that the presence of the quadratic term prevents H to satisfy the passivity condition of the memristor. Indeed, we have

$$H'(\varphi) \geq 0 \, , \quad \forall \varphi \geq \varphi^* \triangleq -\frac{1}{2a}\left(\frac{T}{R_A C} - a + 1\right) \, ,$$

where $\varphi^* < 0$ for $T \geq (a-1) R_A C$. However, if the chaotic motions are known to satisfy a boundedness condition. i.e., $\varphi_k \in [M_i, M_s]$, $M_i < M_s$, $\forall k \in \mathbb{Z}_+$, then it is possible to modify the constitutive relation to make the memristor passive. First, observe that if T satisfies

$$T \geq (a(1-2M_i) - 1)\, R_A C \, , \tag{39}$$

then we have $\varphi^* \leq M_i$ and hence $H'(\varphi) \geq 0$, $\forall \varphi \in [M_i, M_s]$. Now, it is sufficient to find a new function H_p such that $H_p'(\varphi) \geq 0$, $\forall \varphi \in \mathbb{R}$, and $H_p(\varphi) = H(\varphi)$ for $\varphi \in [M_i, M_s]$. For instance, H_p can be chosen as the func-

tion of class $\mathcal{C}^1(\mathbb{R})$ given by

$$H_p(\varphi) = \begin{cases} H(\varphi^*) \text{ if } \varphi < \varphi^* \\ H(\varphi) \quad \text{if } \varphi \geq \varphi^* \end{cases} . \tag{40}$$

Clearly, the DT map obtained by replacing H with H_p exhibits the same dynamic behaviors $\{\varphi_k,\ k \in \mathbb{Z}_+\}$ of (41), whenever $\varphi_k \geq \varphi^*$.

Remark 5 The embedding conditions reported in the third column of Table 1 show that, while the circuit parameters C and R_A are not constrained, the time step T should be sufficiently large, as expected. Indeed, it is bounded below by a quantity proportional to the time constant $R_A C$. The function H defining the constitutive relation of the memristor has a term of the same shape of Φ plus a suitable linear term. In the case of the Logistic Map the function H should be modified to make the memristor passive. Finally, the manifold index ν is either equal to zero or inversely proportional to T, while $\lambda = 1$, i.e., the DT operator is always the Forward Euler Method.

Remark 6 Similar embedding conditions can be developed also for other first-order maps, including the piecewise-linear maps (e.g., Tent Map), the population model (e.g., Ricker Map) and so on [38]. Indeed, it can be readily verified that any first-order state equation of the form $x_{k+1} = G(x_k)$ can be put in the difference equation form (19) by simply setting $z_k = x_k$ and identifying the terms σ_0, z_k, and γ with the linear and the constant terms of the function G, respectively, and Φ with the remaining part of G.

5.2 Derivation of embedding conditions for second-order maps

In this Section, for each second-order map of Table 2 we derive the embedding conditions which are reported in the third column.

5.2.1 Gingerbreadman Map

The difference equation describing this map is given by

$$z_{k+2} + z_k + |z_{k+1}| - 1 = 0$$

and from (26) it follows $\sigma_0 = 1$, $\sigma_1 = 0$, $\Phi = |\varphi|$, and $\gamma = -1$. Hence, equations (30) can be solved only if there exists $\lambda \in (0, 1)$ such that

$$1 = \frac{\lambda - 1}{\lambda} .$$

Consequently, this chaotic map cannot be embedded in the invariant manifolds of the DT memristive cell.

5.2.2 Hénon Map

As shown in Appendix 9, the Hénon Map obeys the following difference equation

$$z_{k+2} - b z_k + \frac{a}{b} z_{k+1}^2 - b = 0 \tag{41}$$

and exhibits quite rich dynamic behaviors when $a > 0$ and $b > 0$, as first observed in [40]. From (26) we have $\sigma_0 = -b$, $\sigma_1 = 0$, $\Phi = (a/b)\varphi^2$, and $\gamma = -b$. In this case, the second equation of (30) is solved for λ such that

$$\lambda = \frac{1}{1+b} . \tag{42}$$

This implies that the embedding equations are solved only if $b > 0$. Setting λ as in (42) with $b > 0$, we can solve the remaining equations of (30) obtaining

$$\begin{aligned} \alpha &= -\frac{C}{T}\frac{1-b}{1+b} - \frac{1}{R_A} , \\ H(\varphi) &= \frac{C}{T}\frac{a}{(1+b)b}\varphi^2 + \left(\frac{C}{T}\frac{1-b}{1+b} + \frac{1}{R_A}\right)\varphi , \\ \nu &= \frac{b}{CT} . \end{aligned}$$

It can be verified that the memristor with the constitutive relation defined by H is not passive since

$$H'(\varphi) \geq 0 , \quad \forall \varphi \geq \varphi^* \triangleq -\frac{b}{2a}\left(1 - b + (1+b)\frac{T}{R_A C}\right) .$$

However, under the assumption that the chaotic motions of interest satisfy $\varphi_k \in [M_i . M_s]$, $M_i < M_s$, $\forall k \in \mathbb{Z}_+$, we can proceed as in the Logistic Map case. Then, we get that it is sufficient to choose T such that

$$T \geq \frac{1}{1+b}\left(\frac{2a}{b} M_i - 1 + b\right) R_A C ,$$

and the function H_p as in (40).

5.2.3 Holmes Map

In this case, the difference equation of the map reads

$$z_{k+2} - d z_{k+1} + b z_k + z_{k+1}^3 = 0 ,$$

thus leading to $\sigma_0 = b$, $\sigma_1 = -d$, $\Phi = |\varphi^3|$, and $\gamma = 0$. In this case the second equation of (30) is satisfied if

$$\lambda = \frac{1}{1-b} , \tag{43}$$

Hence, there exists $\lambda \in (0, 1)$ only for $b < 0$. Unfortunately, this is not true for the usual value (e.g., $b = 0.2$) where the map displays chaotic behaviors.

Employing the expression of λ in (43), the remaining equations of (30) are satisfied for $b < 0$ if

$$\begin{aligned} \alpha &= \frac{d-b-1}{1-b}\frac{C}{T} - \frac{1}{R_A}\,, \\ H(\varphi) &= (1-b)\frac{C}{T}\varphi^3 + \left(\frac{1+b-d}{1-b}\frac{C}{T} + \frac{1}{R_A}\right)\varphi\,, \\ \nu &= 0\,. \end{aligned}$$

Finally, since

$$H'(\varphi) = 3(1-b)\frac{C}{T}\varphi^2 + \left(\frac{1+b-d}{1-b}\frac{C}{T} + \frac{1}{R_A}\right)\,,$$

it follows that the memristor is passive if T satisfies

$$T \geq \frac{d-b-1}{1-b} R_A C\,.$$

5.2.4 Lozi Map

The Lozi Map is a piecewise-linear variation of the Hénon Map that obeys the difference equation

$$z_{k+2} - bz_k + \frac{a}{b}|z_{k+1}| - b = 0$$

and exhibits strange attractors in the so-called Misiurewicz region of the positive quadrant $a > 0$ and $b > 0$ [41]. From (26) we have $\sigma_0 = -b$, $\sigma_1 = 0$, $\Phi = (a/b)\,|\varphi|$, and $\gamma = -b$ which are the same found for the Hénon Map, except for the expression of the function Φ. Hence, it follows that the embedding equations (30) are solved only if $b > 0$ and α, H, and ν are given by

$$\begin{aligned} \alpha &= \frac{a-b-1}{1-b}\frac{C}{T} - \frac{1}{R_A}\,, \\ H(\varphi) &= \frac{C}{T}\frac{a}{(1+b)b}|\varphi| + \left(\frac{C}{T}\frac{1-b}{1+b} + \frac{1}{R_A}\right)\varphi\,, \\ \nu &= \frac{b}{CT}\,. \end{aligned}$$

Furthermore, differently from the Hénon map case, we do not have to modify the shape of H to ensure passivity of the memristor. Indeed, in this case the memristor is passive if the piecewise-linear function H is non-decreasing. It can be readily verified that such a condition holds if T satisfies

$$T \geq \frac{1+a-b^2}{b(1+b)} R_A C\,.$$

Remark 7 Differently form the first-order maps, the embedding conditions are not solvable for all the second-order maps. This is due to the fact that the solution exists only if the second equation of (30) is solvable for some $\lambda \in (0, 1)$, which is equivalent to require that the coefficient σ_0 of (26) is negative. In fact, the Gingerbreadman Map cannot be embedded since $\sigma_0 = 1$. However, it can be possibly embedded if a CT discretization different from (9) is employed. Finally, notice that the considerations in Remark 5 also apply to second-order maps. In particular, to ensure that the memristor is passive in the case of the Hénon Map, the function H should be modified as in the Logistic Map case.

6 Robustness of the embedded dynamics

In Sect. 5 we have derived the conditions for embedding the dynamics of chaotic maps on the invariant manifolds of the DT memristive cell (13). It has been shown that the mixing parameter λ of the DT operator is always equal to 1 for first-order maps, while for second-order maps it depends on some map paramater. The time step T is bounded below by the product of the time constant $R_A C$ and a constant depending on the map parameters, and it influences the function H of the memristor in the circuit of Fig. 1. Furthermore, the index ν of the manifold, where the chaotic dynamics is displayed, is either equal to zero or it depends on some map parameters and T.

In this section we investigate the robustness of the embedded dynamics, i.e., if DT memristive cell displays some attractor on an invariant manifold, then similar attractors are displayed on nearby invariant manifolds. To study this feature we adopt an approach whose main idea can be explained as follows. Consider any chaotic map of those reported in Tables 1 and 2, except for the Gingerbreadman Map that cannot be embedded. Assume that for a given parameter vector ϱ of the difference equation model of the considered map, that is reported in the second column of the Tables, the considered map displays some chaotic attractor and let λ_0, T_0, H_0, and ν_0 satisfy the embedding conditions in the third column of the Tables. Now, suppose that the initialization is not exact, i.e., that the target manifold, actually addressed by the index condition according to (17) or (20), is associated to a different index, namely $\nu = \nu_0 + \delta$, i.e., to an invariant manifold that is close to the target one for small values of δ. This implies that the dynamics on the invariant manifold with index ν is exactly the dynamics of the considered chaotic map where a constant proportional to δ is added to the bias term of the difference equation. By looking at the second column of Tables 1 and 2, it follows that three different cases should be considered: 1) the bias term is equal to zero; 2) the bias term is a component of the vector ϱ that does not affect the

other terms of the map; 3) the bias term is a component of the vector ϱ that affects other terms of the map.

Let us first consider case 2) which concerns the Circle Map and the Gaussian Map. For instance, in the case of the latter map, which obeys the difference equation reported in the second column of Table 1, the bias term is equal to $-c$. Suppose that this difference equation displays a chaotic attractor for given b and c. If λ_0, T_0, H_0, and ν_0 satisfy the embedding conditions in the third column of the Table 1, then this attractor is also displayed on the target manifold with index $\nu_0 = c/T_0$ of the CT memristive cell. It can be readily verified that the dynamics on the manifold of index $\nu = \nu_0 + \delta = c/T_0 + \delta$ obeys the modified difference equation:

$$\varphi_{k+1} - e^{-b\varphi_k^2} - c - T_0\delta = 0 \, .$$

Then, defining

$$\tau(\delta) \triangleq 1 + \frac{T_0}{c}\delta \, ,$$

the above difference equation can be rewritten as

$$\varphi_{k+1} - e^{-b\varphi_k^2} - c^* = 0 \, ,$$

where $c^* = \tau(\delta)c$. This makes it clear that the dynamics of the manifold of index ν is exactly that of the Cubic Map with c replaced by c^*. Since for $\delta \to 0$ we have $\tau(\delta) \to 1$ and so $c^* \to c$, we can conclude that if the parameters b and c are not close to some bifurcation points, then the DT memristive cell displays quite a similar chaotic attractor on nearby invariant manifolds, i.e., with index ν close to ν_0. A similar conclusion applies to the Circle Map.

Consider now case 1) which concerns Cubic, Logistic and Holmes Maps. By reasoning as in case 2), it can be verified that the dynamics on the manifold of index $\nu = \nu_0 + \delta = \delta$ obeys a difference equation having the same terms of the one in the second column of Table 1 with $z_k = \varphi_k$, except for the bias that is equal to $-T_0\delta$. For instance, for the Logistic Map this modified difference equation reads:

$$\varphi_{k+1} - a\varphi_k + a\varphi_k^2 - T_0\delta = 0 \, .$$

Now, consider the new variable

$$\zeta_k \triangleq \frac{\varphi_k - \eta}{\tau}$$

defined via a linear transformation of φ_k where η and τ are fixed later. After some manipulations, the above difference equation can be equivalently rewritten as

$$\zeta_{k+1} - a(1+2\eta)\zeta_k + \tau a\zeta_k^2 + \frac{a\eta^2 + (a-1)\eta - T_0\delta}{\tau} \, . \tag{44}$$

Let $\eta^*(\delta)$ denote the solution of the equation

$$a\eta^2 + (a-1)\eta - T_0\delta = 0$$

such that $\eta^*(0) = 0$. Defining

$$\tau^*(\delta) \triangleq 1 + 2\eta^*(\delta)$$

and setting $\eta = \eta^*(\delta)$, $\tau = \tau^*(\delta)$, the difference equation (44) boils down to

$$\zeta_{k+1}^* - a^*\zeta_k^* + a^*\zeta_k^{*2} = 0 \, ,$$

where $a^* = \tau^*(\delta)a$ and

$$\zeta_k^* \triangleq \frac{\varphi_k - \eta^*(\delta)}{\tau^*(\delta)} \, .$$

Hence, the dynamics on the invariant manifold of intex $\nu = \nu_0 + \delta$ obeys a Logistic Map where a and φ_k are replaced by a^* and ζ_k^*, respectively. Since for $\delta \to 0$ we have $\eta^*(\delta) \to 0$ and $\tau^*(\delta) \to 1$, it follows that $a^* \to a$ and $\zeta_k^* \to \varphi_K$. Hence, we can conclude that if the parameter a of the Logistic Map is not close to some bifurcation points, then the DT memristive cell displays similar chaotic attractors on nearby invariant manifolds. Similar conclusions hold for the Cubic and Holmes Maps.

Finally, consider case 3) which concerns the Hénon Map and the Lozi Map. By reasoning as in the previous cases, we can show that the dynamics on the manifold of index $\nu = \nu_0 + \delta = b/((1-b)T_0) + \delta$ obeys a difference equation having the same terms of the one in the second column of Table 1 with $z_k = \varphi_k$, except for the bias term that is equal to $-b - T_0\delta$. For instance, for the Hénon Map this modified difference equation is given by:

$$\varphi_{k+2} - b\varphi_k + \frac{a}{b}\varphi_{k+1}^2 - b - T_0(1-b)\delta = 0 \, .$$

As in case 1), we define a new variable via a linear transformation of the variable φ_k. Specifically, we define

$$\zeta_k \triangleq \frac{\varphi_k}{\tau}$$

where τ is fixed later. Then, the above difference equation can be rewritten in the following equivalent form

$$\zeta_{k+2} - b\zeta_k + \frac{\tau a}{b}\zeta_{k+1}^2 - \frac{b + T_0(1-b)\delta}{\tau} = 0 \, . \tag{45}$$

Defining the function

$$\tau^*(\delta) = 1 + \frac{1-b}{b} T_0 \delta \,,$$

and setting $\tau = \tau^*(\delta)$, the difference equation (45) becomes

$$\zeta^*_{k+2} - b\zeta^*_k + \frac{a^*}{b}\zeta^{*2}_{k+1} - b = 0 \,,$$

where $a^* = \tau^*(\delta)a$ and

$$\zeta^*_k \triangleq \frac{\varphi_k}{\tau^*(\delta)} \,.$$

Therefore, on the invariant manifold of intex $\nu = \nu_0 + \delta$ the dynamics is governed by the Hénon Map with a^* and ζ^*_k in place of a and φ_k, respectively. Clearly, for $\delta \to 0$ it follows that $\tau^*(\delta) \to 1$ and so $a^* \to a$ and $\zeta^*_k \to \varphi_K$. Hence, as in the previous cases, we can conlude that quite similar attractors are displayed on nearby invariant manifolds if the embedded Hénon Map is not close to some bifurcation phenomena. A similar conclusion applies to the Lozi Map.

Summing up, we have shown that that if some attractor is embedded on an invariant manifold with index ν_0 of DT memristive cell (13), then a similar attractor is displayed on invariant manifolds with index ν close to ν_0. This robustness of the embedded dynamics is a consequence of the foliation feature that naturally leads to the coexistence of infinitely many convergent, oscillatory and chaotic behaviors, a peculiar property often termed as extreme multistability.

7 Numerical example and discussion of the results

The procedure exemplified in Sect. 5 is conceived to embed complex maps into a manifold dynamics of the DT memristive cell described by the difference equation (13). As previously discussed, this requires to satisfy a number of conditions that for the maps considered in this paper have been reported in Tables 1 and 2. The constraints regard two crucial aspects: the configuration of the CT circuit, and precisely of the nonlinear characteristic function H of the memristor, that must also be passive; and the discretization method, in terms of both the step T and the mixing parameter λ. Moreover, as discussed in Sect. 6, the embedded dynamics must be triggered by initializing the DT cell onto the right manifold, under the assurance that small deviations from the correct value of the index ν can be tolerated as much as the sought complex behavior is far from bifurcations able to disrupt the desired regime.

In this section, we will illustrate in detail how to design the CT circuit so that the corresponding DT cell is able to mimic the Logistic Map.

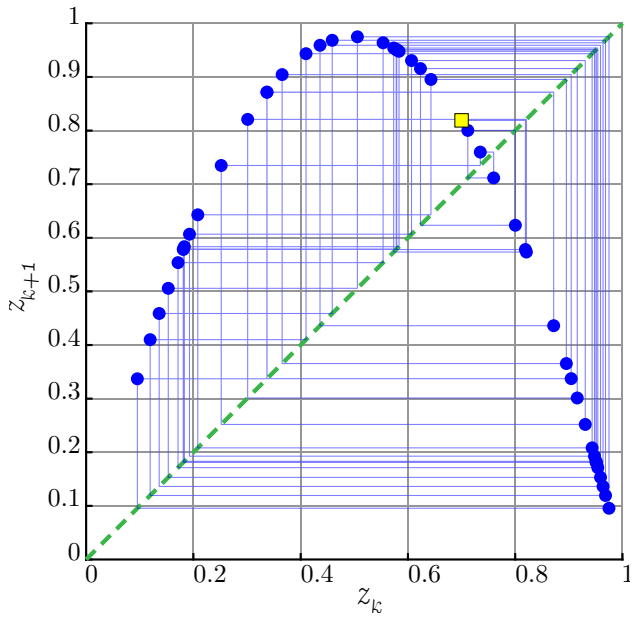

Fig. 2 First-return map of the Logistic Map. The map is initialized at the first time step in $z_1 = 0.7$. The yellow square marks the related (z_1, z_2), corresponding to the first iteration of the first-return map

The first step in this process is setting up the values of R_A and C, because they are not subject to any constraints. For the sake of the simplicity, let us assume that they are unitary in normalized units of measure:

$$C = 1 \,, \quad R_A = 1$$

As second step, one must decide the behavior to embed, thus fixing the bifurcation parameter of the Logistic Map. Our choice is $a = 3.9$, instead of the more usual $a = 4$, because it is not located at the edge of the chaotic region, thus guaranteeing a neighboring safe region where the dynamics does not change its nature after small perturbations of the parameter. This is crucial regarding the robustness of the DT cell dynamics against inaccurate starting conditions, as discussed in Sect. 6. The first-return map of the Logistic Map (35) for $a = 3.9$ is depicted in Fig. 2 for the initial condition $z_1 = 0.7$, while its bifurcation diagram with respect to the same parameter is reported in Fig. 3.

In the third step, T is chosen to meet the requirement in (39), also reported in Table 1. From the bifurcation diagram of the Logistic Map, a boundedness condition valid not only at $a = 3.9$ but in a wider region around it, is $[M_i, M_s] = [0, 1]$. Thus, the discretization step must be set so that

$$T \geq 2.9 \tag{46}$$

Finally, the nonlinearity H must satisfy both the condition in (37) and the passivity property. Therefore, following the reasoning illustrated in Sect. 5.1.4, its implementation can be performed using its passive extension:

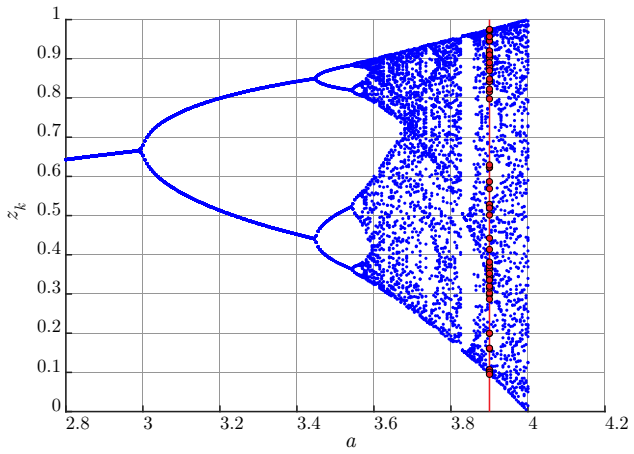

Fig. 3 Bifurcation diagram of the Logistic Map against parameter a. For each value of a, the diagram plots 50 points visited by the map after discarding a transient of 200 time steps. The dynamics selected for the DT cell corresponds to the red dots at $a = 3.9$

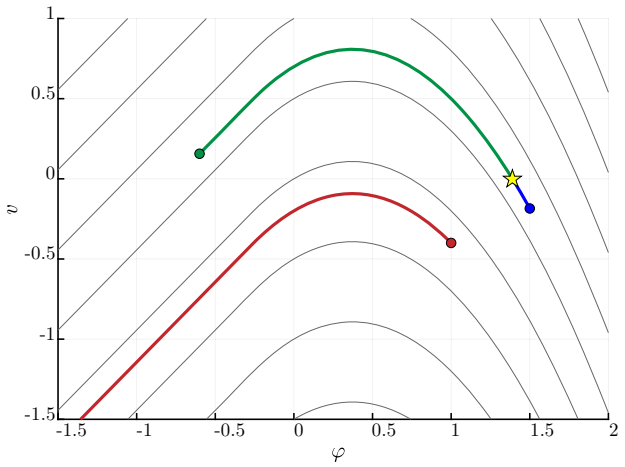

Fig. 4 State space (φ, v) of the CT cell using the nonlinear function (47) with $T = 5$. The solid grey lines illustrate a selection of reference invariant manifolds. The solid blue, green, and red lines depict three different trajectories starting from the dots of the corresponding color. The blue and green trajectories lie on the same one-dimensional manifold and converge to the same equilibrium point (marked using the star symbol). The red trajectory diverges

$$H_p(\varphi) = \begin{cases} -\frac{T}{15.6}\left(1 - \frac{2.9}{T}\right)^2 \\ \qquad \text{if } \varphi < -\frac{T}{15.6}\left(1 - \frac{2.9}{T}\right) \\ \frac{3.9}{T}\varphi^2 + \left(1 - \frac{2.9}{T}\right)\varphi \\ \qquad \text{if } \varphi \geq -\frac{T}{15.6}\left(1 - \frac{2.9}{T}\right) \end{cases} . \tag{47}$$

This way the configuration and the implementation of both the CT circuit and the DT cell are almost done, except for the discretization step T, that notably affects them both. Figures 4 and 5 depicts three different trajectories of the CT circuit obtained using $T = 5$, which satisfies (46). To highlight the foliation property and the coexistence of manifolds characterized by their own dynamics, the presented solutions have been chosen to feature two trajectories taken on the same manifold and converging to the same equilibrium point, and a diverging one on a different manifold.

As discussed in Sect. 4, the embedding of first order maps implies taking $\lambda = 1$ (see also Table 1). Therefore, given the previous requirements, the difference equation (13) of the corresponding DT map is

$$\frac{h-1}{T}\left(\frac{h-1}{T}\varphi_k - \varphi_k + H_p(\varphi_k)\right) = 0 , \tag{48}$$

which boils down to the explicit form

$$\varphi_{k+2} - (2 + T^2)\varphi_{k+1} + (1 + T^2)\varphi_k + T^2 H_p(\varphi_{k+1}) - T^2 H_p(\varphi_k) = 0 .$$

The common state space representation of the above map is obtained defining $\hat{z}_{1,k} \triangleq \varphi_k$ and $\hat{z}_{2,k} \triangleq \varphi_{k+1}$, so that:

$$\begin{cases} \hat{z}_{1,k+1} = \hat{z}_{2,k} \\ \hat{z}_{2,k+1} = -\left(1 + T^2\right)\hat{z}_{1,k} + \left(2 + T^2\right)\hat{z}_{2,k} \\ \qquad + T^2 H_p(\hat{z}_{1,k}) - T^2 H_p(\hat{z}_{2,k}) \end{cases} , \tag{49}$$

Observe that the term in the brackets in (48) is both the equation of the reduced order invariant manifold (25) discussed in Sect. 3

$$z_{2,k} - (1 + T)\, z_{1,k} + T\, H_p(z_{1,k}) = T\nu$$

and the equation (19) that describes the dynamics on the same invariant manifold of index ν:

$$\varphi_{k+1} = (1 + T)\,\varphi_k - T\, H_p(\varphi_k) + T\nu .$$

Notice that index ν depends on the initial conditions $(\varphi_0, \varphi_1) = (\hat{z}_{1,0}, \hat{z}_{2,0})$ according to (20), while $H_p(\varphi)$ in (47) has been designed to depend on T to guarantee passivity, as explained in Sect. 5.1.4 (see also (40)).

To exemplify the embedding capability of the DT cell, two different values of T satisfying (46) have been chosen: $T_1 = 5$, and $T_2 = 20$. In order to trigger the embedded Logistic Map, the starting condition must lie onto the manifold of index $\nu = \nu_0 \triangleq 0$, as reported in Table 1. Hence, to exactly induce the same dynamics exhibited in Fig. 2, it is necessary to set $\varphi_1 = \hat{z}_{2,0} = z_1$, the latter being the coordinate of the reference Logistic Map. Since the DT cell (13) is a second order difference equation, the initial value φ_0 of the sequence

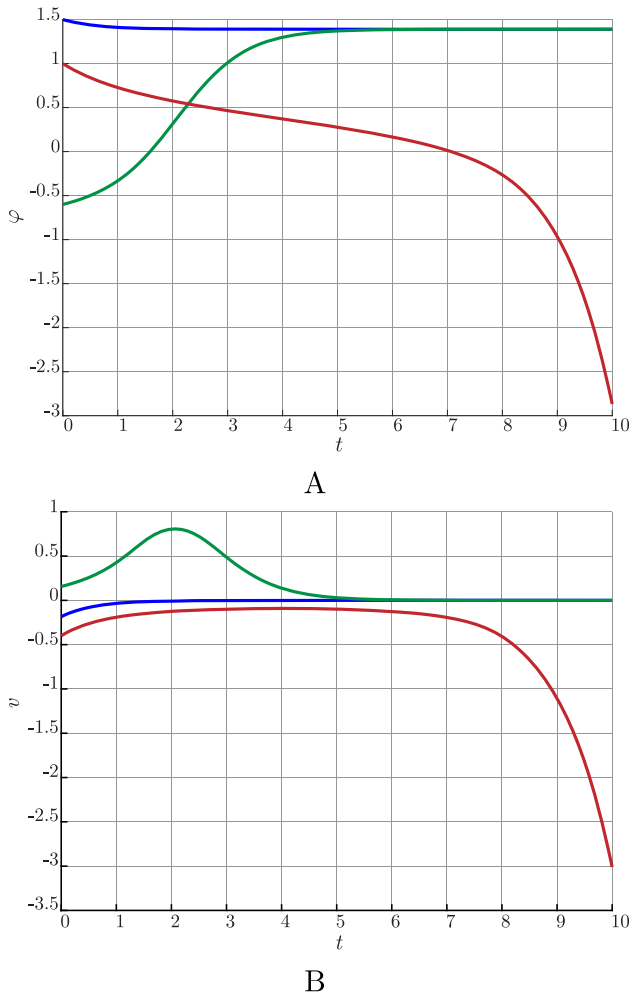

Fig. 5 Temporal evolution of the coordinates φ (A) and v (B) of the CT cell used in Sect. 7. The three solutions correspond to the trajectories of the same color depicted in Fig. 5

can be chosen equal to

$$\varphi_0 = \hat{z}_{1,0} = \frac{1}{2}\left(1 + \sqrt{1 - \frac{4}{a} z_1}\right)$$

so to satisfy the manifold index equation (20). As expected, substituting T_1 and T_2 in the above equation and initializing the DT cell at the corresponding starting conditions, in both the cases it exactly exhibits the same dynamics of the Logistic Map. The first-return map obtained for both T_1 and T_2 is reported in Figures 6, and a direct comparison with Fig. 2 is sufficient to prove the perfect embedding of the chaotic map. It is worth stressing that the steps T satisfying (46) define a family of CT circuits and related DT cells, which are different, but still all of them are able to display the same Logistic Map on their manifolds with index ν_0. Indeed, the DT cells obtained using the above T_1 and T_2 are different systems, because the nonlinear function (47) depends on the

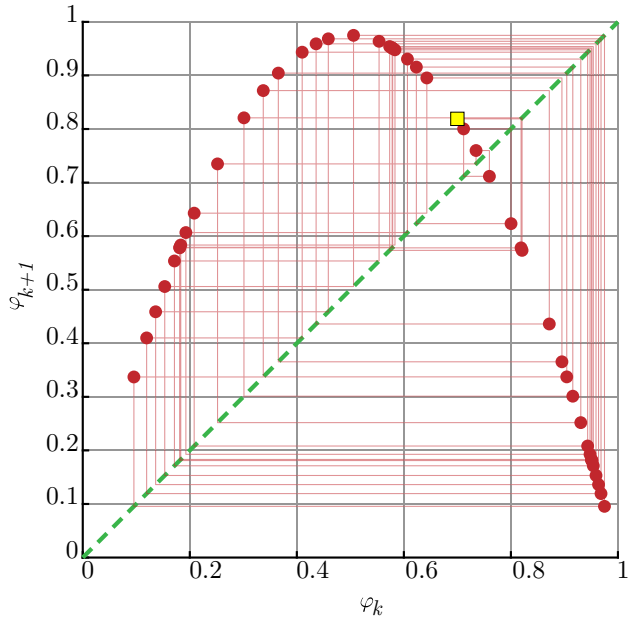

Fig. 6 First-return map exhibited on the manifold ν_0 by the DT cell of Sect. 7 when $T = 5$ and $T = 20$, but not limited to these cases only. In fact, this return map is shown for all the T's satisfying condition (46). The yellow square denotes the initial condition on the manifold, that is the same used for the Logistic Map of Fig. 2

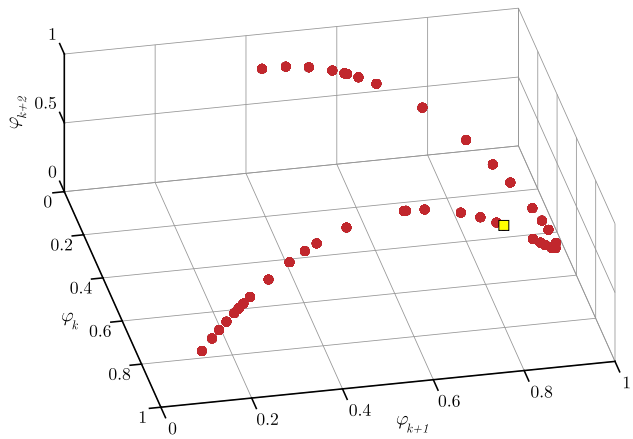

Fig. 7 Second-return map of the DT cell of Sect. 7 initialized on manifold ν_0 for $T = 5$ and $T = 20$. The two return maps are coincident. Moreover, the same map is exhibited for all the T satisfying condition (46). The yellow square denotes the initial condition corresponding the starting point on the manifold shown in Fig. 6

actual value of T. Nonetheless, on the manifolds ν_0 they exhibit the same complete dynamics, as illustrated in Fig. 7 where the second-return map featured by both the DT cells is reported.

Finally, to verify the robustness of the DT cell against initialization errors, we fix a proper discretization step T and vary the starting point $(\varphi_0, \varphi_1) = (\hat{z}_{1,0}, \hat{z}_{2,0})$ according to the equations

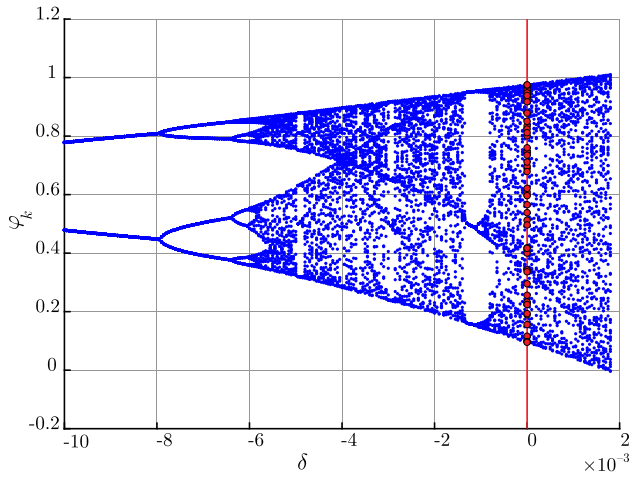

Fig. 8 Bifurcation diagram of the DT cell described in Sect. 7, plotted against initial conditions lying on the manifolds $\nu = \delta$ with $\delta \in [-0.0100, 0.0018]$ for fixed $\varphi_1 = 0.7$. The red dots correspond to the Logistic Map dynamics on the manifold ν_0

$$\varphi_0 = \hat{z}_{1,0} = \frac{1}{2}\left(1 + \sqrt{1 - \frac{4}{a}z_1 + 4T\delta}\right) \tag{50}$$

$$\varphi_1 = \hat{z}_{2,0} = z_1 \tag{51}$$

for δ spanning an interval around zero. From equation (20) it follows that this choice of the initial conditions sets the starting point of the DT cell on the manifold with index $\nu = \delta$. Thus, by varying δ the behaviors on the neighboring manifolds around ν_0 are scanned, while keeping the starting condition on the manifold itself always fixed at $\varphi_1 = z_1$. The results are presented in Fig. 8 in the form of a bifurcation diagram to clarify that around the desired dynamics there are infinite similar chaotic behaviors. Since different values of δ, according to (50)-(51), generate different initial conditions of the DT map, the same figure also demonstrates the coexistence of an infinite number of attractors for the same fixed configuration of the DT map, or in other words the "extreme multistability" of the model. In order to clarify how coexisting chaotic attractors are placed within the state space of the map, two neighboring dynamics related to $\nu = -0,0024$ and $\nu = 0.0012$ are depicted in Fig. 9 in comparison with the Logistic Map featured at $\nu = 0$. Notice that the embedding value $\nu = 0$ corresponds in this example to $a = 3.9$, and, therefore, as explained in Sect. 6, small perturbation of the initial conditions are equivalent to variation of the Logistic Map's bifurcation parameter. Such a feature is crucial for the resilience of the dynamics.

7.1 Final Remarks

The illustrative example discussed above demonstrates that, starting from a simple CT memristive cell, it is possible to

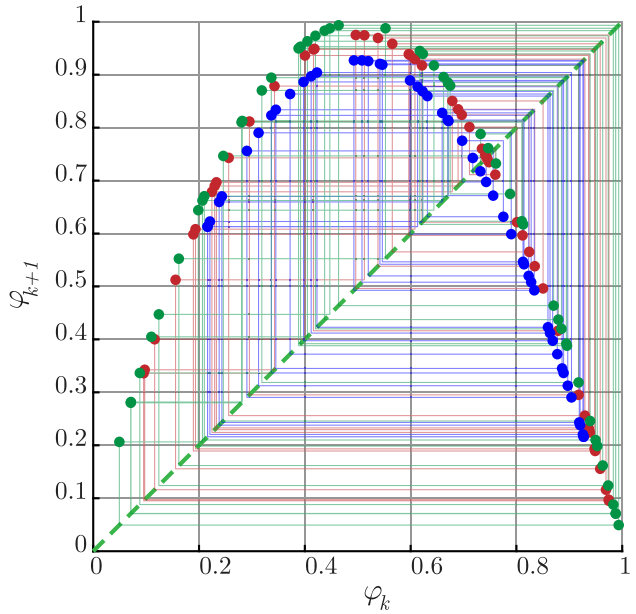

Fig. 9 First-return maps of the dynamics of Fig. 8 at $\nu = -0.0024$ (blue dots), $\nu = 0$ (red dots), and $\nu = 0.0012$ (green dots)

derive a DT memristive model with a foliated state space that successfully embeds the chaotic Logistic Map on a specific invariant manifold. This chaotic dynamics is not merely a localized phenomenon. Rather, it exhibits a robustness to initialization errors that is functionally equivalent to the robustness of the original Logistic Map within its chaotic parameter range. Notably, our analysis highlights that the DT memristive map possesses an infinite number of non-isolated chaotic attractors distributed across adjacent invariant manifolds. This structural complexity makes the system an ideal candidate for high-throughput pseudo-random number generation and secure encryption applications. In this regard, the inherent simplicity of the state equations (49) and the straightforward nature of the nonlinear characteristic function (47) render both software and hardware implementations (e.g., on FPGA or DSP platforms) highly efficient, offering a low-complexity alternative to traditional chaotic generators.

Furthermore, the bifurcation diagram, presented in Figure 8 and plotted against the initial conditions which activate the specific invariant manifold and are equivalent to varying the index ν, reveals that the same DT map supports a rich coexistence of non-chaotic attractors, including stable limit cycles and fixed points (placed at lower values with respect to the actually plotted range of δ). Such a dynamical diversity could be strategically exploited to enhance the computational repertoire of reservoir computing systems. Specifically, the vast plethora of available behaviors could serve as a rich "dictionary" for temporal signal processing, where a high variety of baseline responses is essential for effective classification and prediction. Even in this context, the extreme constructive

simplicity of the model remains a key factor in increasing the overall efficiency and scalability of the implementation.

8 Conclusions

This paper has developed a design framework for creating discrete-time (DT) memristive maps aimed at preserving the fundamental foliation property of the original inspiring continuous-time (CT) circuits. Furthermore, it has investigated how the choice of the discretization operator and the related time step can be leveraged to finely tune the resulting dynamics, enabling the "embedding" of complex behaviors that are not exhibited in the original CT circuit. To illustrate this methodology, the paper considered a CT memristor-capacitor circuit, i.e, the parallel interconnection of a capacitor, a passive ideal flux-controlled memristor and an active resistor. It is known that such a circuit possesses only equilibrium points as attractors and it enjoys the *foliation feature*, i.e., each circuit solution is constrained to evolve on one of the infinitely many invariant manifolds that make up the state space. A DT map is derived from this circuit via a discretization procedure based on mixing Forward and Backward Euler methods. Such a DT map is described by a difference equation model that depends on the discretization time step T and the mixing parameter λ, and it preserves the foliation feature for any $T > 0$ and any $\lambda \in [0, 1]$. Then, it is shown that the dynamics of some well-known first-order and second-order chaotic maps can be exactly reproduced on some invariant manifolds of the derived DT map, if some embedding conditions are satisfied. Notably, these conditions are solved for any first-order map with $\lambda = 1$ (i.e., Forward Euler method) and some second-order maps (e.g., Hénon Map, Lozi Map) with $\lambda \in (0, 1)$ if T is larger than a quantity proportional to the time constant of the CT memristor-capacitor circuit.

The proposed design framework can offer significant advantages for practical applications. First, it enables the creation of complex maps using simple, non-periodic nonlinearities, effectively avoiding the use of trigonometric functions (such as sine or cosine). While these functions are commonly exploited in existing DT memristive systems to enforce complex dynamics via an infinite number of isolated fixed points, they are computationally expensive to implement in digital electronic hardware. Therefore, they do not represent an efficient solution for generating complexity. In contrast, our results demonstrate that chaotic behaviors and the coexistence of attractors can be successfully induced in DT models without resorting to trigonometric functions, thanks to the preserved foliation property and the flexibility in map design guaranteed by the broad choice of discretization operators, here represented by the mixing coefficient λ. Notice also that, if the embedding requires a specific value of λ, it implies that the desired dynamics can only be achieved using a certain discretization operator, thus highlighting its critical importance. Hence, these DT maps can show the coexistence of infinitely many convergent, oscillatory and chaotic behaviors, i.e., extreme multistability, even when the only attractors of the CT circuit are equilibrium points. To illustrate the discretization procedure and the derivation of the embedding conditions, the Logistic Map has been considered in detail.

Furthermore, another significant advantage of the proposed approach is the robustness property enjoyed by the derived DT maps, i.e., if some attractor is displayed on an invariant manifold of the map, then similar attractors are displayed on nearby invariant manifolds. This resilience ensures that the resulting behavior remains robust against inevitable numerical approximations. Since practical implementations, whether as software algorithms or via digital hardware, are subject to the inaccuracies of a finite-precision arithmetic, this property is crucial in real-world applications.

At least two directions for future research can be identified. The first is to investigate more general discretization operators capable of preserving the foliation property. This would allow the DT maps derived from the CT memristor-capacitor circuit to incorporate the dynamics of a broader class of second-order and higher-order chaotic or hyperchaotic maps, further enhancing the "versatility" of the proposed cell. Such increased flexibility is particularly promising for pseudo-random number generation and its primary applications, such as image encryption, where higher security standards must be met while maintaining low implementation costs. The second direction concerns the role of the discretization operator in generating complex dynamics when the CT memristor-capacitor circuit is equipped with a real memristor rather than an ideal one. This approach could provide a framework to investigate physical phenomena such as energy dissipation, which can significantly alter the foliation property without completely destroying it (see [9]). This may lead to the development of complex dynamics in the resulting DT maps, characterized by behaviors fundamentally different from those observed in the ideal case.

9 Appendix: Difference equation model of second-order chaotic maps

In this Appendix the derivation of the difference equation model is illustrated for the Hénon map. The difference equations of the other second-order maps reported in Table 2 can be readily obtained by proceeding in the same way.

We first rewrite the state equations of the Hénon Map (see the first column of Table 2) as

$$\begin{cases} hx_k = 1 - ax_k^2 + y_k \\ hy_k = bx_k \, . \end{cases} \tag{52}$$

Then, assuming $b \neq 0$, we solve for x_k the second equation, i.e., $x_k = \frac{1}{b} h y_k$, and substitute into the first one, thus obtaining

$$\frac{1}{b} h^2 y_k - y_k + \frac{a}{b^2} h y_k^2 - 1 = 0 \, .$$

Rearranging the terms, we get the final form of the difference equation

$$y_{k+2} - b y_k + \frac{a}{b} y_{k+1}^2 - b = 0 \, ,$$

which is the one reported in the second column of Table 2, once we set $y_k = z_k$.

Author Contributions G.I. and A.T. contributed to the conceptualization of the work, developed the methodology, and wrote the original draft. M.D.M., L.P., and M.F. reviewed and edited the final manuscript.

Funding Open access funding provided by Università degli Studi di Firenze within the CRUI-CARE Agreement. The authors declare that no funds, grants, or other support were received during the preparation of this manuscript.

Data Availability The numerical data supporting this study were generated based on the algorithms outlined herein. Detailed simulation parameters can be provided by the corresponding author upon reasonable request.

Declarations

Competing Interests The authors declare no competing interests.

References

1. Strukov, D.B., Snider, G.S., Stewart, D.R., Williams, R.S.: The missing memristor found. Nature **453**(7191), 80 (2008)
2. Chua, L.O.: Memristor-The missing circuit element. IEEE Trans. Circuit Theory **18**(5), 507–519 (1971)
3. Itoh, M., Chua, L.O.: Memristor oscillators. International Journal on Bifurcations and Chaos **18**(11), 3183–3206 (2008)
4. Muthuswamy, B., Kokate, P.P.: Memristor-based chaotic circuits. IETE Tech. Rev. **26**(6), 417–429 (2009)
5. Driscoll, T., Pershin, Y., Basov, D., Di Ventra, M.: Chaotic memristor. Applied physics A **102**(4), 885–889 (2011)
6. Kumar, S., Strachan, J.P., Williams, R.S.: Chaotic dynamics in nanoscale NbO2 Mott memristors for analogue computing. Nature **548**, 318–321 (2017). https://doi.org/10.1038/nature23307
7. Sun, J., Zhao, X., Fang, J., Wang, Y.: Autonomous memristor chaotic systems of infinite chaotic attractors and circuitry realization. Nonlinear Dyn. **94**(4), 2879–2887 (2018)
8. Corinto, F., Forti, M., Chua, L.O., et al.: Nonlinear circuits and systems with memristors. Springer, Cham, Switzerland (2021)
9. Innocenti, G., Tesi, A., Di Marco, M., Forti, M.: First integrals can explain coexistence of attractors, multistability, and loss of ideality in circuits with memristors. Chaos, Solitons Fractals **180**, 114504 (2024). https://doi.org/10.1016/j.chaos.2024.114504
10. Hens, C.R., Banerjee, R., Feudel, U., Dana, S.K.: How to obtain extreme multistability in coupled dynamical systems. Phys. Rev. E **85**, 035202 (2012). https://doi.org/10.1103/PhysRevE.85.035202
11. Bao, B.-C., Xu, Q., Bao, H., Chen, M.: Extreme multistability in a memristive circuit. Electron. Lett. **52**(12), 1008–1010 (2016)
12. Corinto, F., Forti, M.: Memristor Circuits: Bifurcations without Parameters. IEEE Trans. Circuits Syst. I, Reg. Papers 64(6), 1540–1551 (2017)
13. Chang, H., Li, Y., Yuan, F., Chen, G.: Extreme multistability with hidden attractors in a simplest memristor-based circuit. International Journal of Bifurcation and Chaos **29**(06), 1950086 (2019). https://doi.org/10.1142/S021812741950086X
14. Itoh, M., Chua, L.: Memristor Cellular Automata and Memristor Discrete-Time Cellular Neural Networks, pp. 1289–1361. Springer, Cham (2019)
15. Solan, E., Ochs, K.: Wave digital emulation of general memristors. Int. J. Circuit Theory Appl. **46**(11), 2011–2027 (2018)
16. Xu, B., Zou, S., Bai, L., Chen, K., Zhao, J.: A general discrete memristor emulator based on taylor expansion for the reconfigurable fpga implementation and its application. Nonlinear Dyn. **112**(2), 1395–1414 (2024)
17. Bao, B.-C., Li, H., Wu, H., Zhang, X., Chen, M.: Hyperchaos in a second-order discrete memristor-based map model. Electron. Lett. **56**(15), 769–770 (2020). https://doi.org/10.1049/el.2020.1172
18. Peng, Y., Sun, K., He, S.: A discrete memristor model and its application in Hénon map. Chaos, Solitons & Fractals **137**, 109873 (2020)
19. Li, H., Hua, Z., Bao, H., Zhu, L., Chen, M., Bao, B.: Two-dimensional memristive hyperchaotic maps and application in secure communication. IEEE Trans. Industr. Electron. **68**(10), 9931–9940 (2020)
20. Bao, H., Hua, Z., Li, H., Chen, M., Bao, B.: Discrete memristor hyperchaotic maps. IEEE Trans. Circuits Syst. I Regul. Pap. **68**(11), 4534–4544 (2021)
21. Deng, Y., Li, Y.: Nonparametric bifurcation mechanism in 2-D hyperchaotic discrete memristor-based map. Nonlinear Dyn. **104**(4), 4601–4614 (2021)
22. Zhang, S., Zhang, H., Wang, C.: Dynamical analysis and applications of a novel 2-D hybrid dual-memristor hyperchaotic map with complexity enhancement. Nonlinear Dyn. **111**(16), 15487–15513 (2023)
23. He, S., Zhan, D., Wang, H., Sun, K., Peng, Y.: Discrete memristor and discrete memristive systems. Entropy **24**(6), 786 (2022)
24. Ma, M., Yang, Y., Qiu, Z., Peng, Y., Sun, Y., Li, Z., Wang, M.: A locally active discrete memristor model and its application in a hyperchaotic map. Nonlinear Dyn. **107**(3), 2935–2949 (2022)

25. He, S., Liu, J., Wang, H., Sun, K.: A discrete memristive neural network and its application for character recognition. Neurocomputing **523**, 1–8 (2023)
26. Wang, C., Chong, Z., Zhang, H., Ma, P., Dong, W.: Color image encryption based on discrete memristor logistic map and dna encoding. Integration **96**, 102138 (2024)
27. Deng, Y., Zhang, S., Yuan, F., Li, Y., Wang, G.: Reservoir computing system using discrete memristor for chaotic temporal signal processing. Chaos, Solitons & Fractals **194**, 116230 (2025). https://doi.org/10.1016/j.chaos.2025.116230
28. Lin, Z., Deng, J., Chen, Z., Zhang, J., Liang, S., Feng, Y.: An efficient reservoir computing system based on 2D mask processing and dynamic memristor: Z. lin et al. Nonlinear Dynamics 113(15), 20191–20209 (2025)
29. Hussan, I., Zhao, M., Zhang, X.: Two-memristor-based maps with infinitely many hyperchaotic attractors. Chaos, Solitons & Fractals **191**, 115904 (2025)
30. Di Marco, M., Forti, M., Pancioni, L., Tesi, A.: New class of discrete-time memristor circuits: first integrals, coexisting attractors and bifurcations without parameters. International Journal of Bifurcation and Chaos **34**(01), 2450001 (2024)
31. Di Marco, M., Forti, M., Pancioni, L., Tesi, A.: Snap-back repellers and chaos in a class of discrete-time memristor circuits. Nonlinear Dyn. **112**(15), 13519–13537 (2024)
32. Di Marco, M., Forti, M., Pancioni, L., Innocenti, G., Tesi, A.: Embedding classic chaotic maps in simple discrete-time memristor circuits. IEEE Access (2024)
33. Innocenti, G., Tesi, A., Di Marco, M., Pancioni, L., Mauro, F.: Feature preserving discretization of memristive circuits using an input-output approach. Nonlinear Dynamicss **113**, 8179–28206 (2025). https://doi.org/10.1007/s11071-025-11568-4
34. Lorenz, E.N.: Computational chaos-a prelude to computational instability. Physica D **35**(3), 299–317 (1989)
35. Atkinson, K.E.: An Introduction to Numerical Analysis. John Wiley & Sons, New York, US (2008)
36. Butcher, J.C.: Numerical Methods for Ordinary Differential Equations. John Wiley & Sons, Chichester, UK (2016). https://doi.org/10.1002/9781119121534
37. Leader, J.J.: Numerical Analysis and Scientific Computation. Chapman and Hall/CRC, New York, US (2022)
38. Sprott, J.C.: Chaos and Time-series Analysis. Oxford University Press, Oxford, UK (2003). https://doi.org/10.1093/oso/9780198508397.001.0001
39. Hilborn, R.C.: Chaos and Nonlinear Dynamics: an Introduction for Scientists and Engineers. Oxford University Press, New York, US (2000)
40. Hénon, M.: A two-dimensional mapping with a strange attractor. Commun. Math. Phys. **50**(1), 69–77 (1976)
41. Lozi, R.: Survey of recent applications of the chaotic Lozi map. Algorithms **16**(10), 491 (2023)